

46

NASA TECHNICAL  
MEMORANDUM

NASA TM X-53089

JULY 27, 1964

NASA TM X-53089

FACILITY FORM 602	<u>N64-31549</u>	<u>                    </u>
	(ACCESSION NUMBER)	(THRU)
	<u>46</u>	<u>1</u>
	(PAGES)	(CODE)
	<u>TMX-53089</u>	<u>04</u>
	(NASA CR OR TMX OR AD NUMBER)	(CATEGORY)

# STUDY OF SPHERE MOTION AND BALLOON WIND SENSORS

by PAUL B. MacCREADY, JR. AND HENRY R. JEX\*  
For Aero-Astroynamics Laboratory

\*Prepared by Meteorology Research, Inc.

NASA

*George C. Marshall  
Space Flight Center,  
Huntsville, Alabama*

## OTS PRICE

XEROX	\$	<u>2.00 FS</u>
MICROFILM	\$	<u>0.50 mf.</u>

-----

## FOREWORD

This report presents the results of a study performed by Meteorology Research, Inc., Altadena, California as part of NASA Contract NAS8-5294 with the Aero-Astrophysics Office, Aero-Astrodynamics Laboratory, NASA-George C. Marshall Space Flight Center, Huntsville, Alabama. The NASA contract monitor was Mr. James R. Scoggins; Dr. Paul B. MacCready was the principal investigator.

The results of this study improve considerably our understanding of the behaviour of spheres moving through a fluid, but much remains to be done before a complete understanding is achieved. Further work is being done as part of this contract, while different approaches are being followed at the Marshall Space Flight Center, Langley Research Center, Air Force Cambridge Research Laboratories, and elsewhere.

The contract period covered by this portion of the contract was April 1963 to April 1964.

**CASE COPY**

13444

TECHNICAL MEMORANDUM X-53089

STUDY OF SPHERE MOTIONS AND BALLOON WIND SENSORS<sup>1</sup>

By

Paul B. MacCready, Jr.<sup>2</sup>

and

Henry R. Jex<sup>3</sup>

ABSTRACT

31549

Balloons ascending in still air typically exhibit lateral movements which introduce errors when the balloons are tracked as sensors of wind motion. This report examines some of the fundamentals of the fluid flows and associated motions and net drag coefficients of free-moving spheres. The flows and motions depend directly on Reynolds number ( $R_d$ ) which determines the flow regime; depend on the relative mass of the sphere to the fluid it displaces (RM) because, for a given  $R_d$ , the lower the RM values the greater the lateral motions and thus the larger the total wake size and drag; and also depend on the sphere rotational inertia and minute details of surface roughness, sphericity, and random orientation. Because of these complex interactions no unique drag coefficient ( $C_D$ ) vs  $R_d$  curve can be found for free-moving spheres. The separate effects of the main factors are described as they might affect an idealized  $C_D$  vs  $R_d$  curve for a perfectly smooth free-moving sphere of infinite RM.

*Author*

<sup>1</sup>This study was performed by Meteorology Research, Inc., Altadena, California, as part of NASA Contract NAS8-5294 with the Aero-Astrodynamic Laboratory, Aero-Astrophysics Office, Marshall Space Flight Center, Huntsville, Alabama. Final Report MR164 FR-147, April 1964.

<sup>2</sup>Meteorology Research, Inc.

<sup>3</sup>Systems Technology, Inc., Inglewood, California, as consultant to Meteorology Research, Inc.

Observations were made of the mean vertical velocity and the magnitude of the lateral motions as spherical balls and balloons ascended and descended through both water and air, covering wide ranges of  $R_d$  and  $RM$ . The results are in general agreement with the physical concepts developed, and the water experiments give results consistent with the tests in air. In the subcritical  $R_d$  regime, where the wake separation is laminar, the motion tends to be a fairly regular zigzag, or spiral, of wave length on the order of 12 times the diameter. The magnitude of the lateral motion is roughly related to the factor  $(1 + 2RM)^{-1}$ . In the supercritical  $R_d$  regime, where the wake separation is turbulent and the wake is smaller, the motion tends to be an irregular meandering spiral. In the critical range of  $R_d$  the shift from subcritical to supercritical (and vice versa) flows and drags is rather abrupt; if sufficiently abrupt, there is a hysteresis effect with increasing and decreasing Reynolds number, and two stable velocities exist.

Tests were also made in air with spheres to which skirts, vanes, and/or drag chutes were affixed in an effort to stabilize the motion.

It is concluded that balloon motion can be smooth enough for most needs for high resolution atmospheric wind data if spherical or semi-spherical balloons are used operating always in the subcritical range, or certain balloons are used with roughness elements or other attachments operating at even higher Reynolds numbers.

NASA-GEORGE C. MARSHALL SPACE FLIGHT CENTER

---

TECHNICAL MEMORANDUM X-53089

---

July 27, 1964

STUDY OF SPHERE MOTION AND BALLOON WIND SENSORS

By

Paul B. MacCready, Jr.

and

Henry R. Jex

prepared by  
Meteorology Research, Inc.

for

Aero-Astrophysics Office  
Aero-Astrodynamic Laboratory

## TABLE OF CONTENTS

	Page
SUMMARY	1
I. INTRODUCTION	3
II. DEFINITIONS AND RELATIONSHIPS	5
III. FORCES AND FLUID MOTIONS FOR FIXED AND FREELY MOVING SPHERES	7
IV. THE RELATIVE MASS EFFECT	16
V. OPERATION IN THE CRITICAL RANGE OF REYNOLDS NUMBER	20
VI. EXPERIMENTAL RESULTS AND INTERPRETATIONS	24
VII. CONCLUSIONS AND RECOMMENDATIONS	35
ACKNOWLEDGMENTS	37
REFERENCES	38

## LIST OF ILLUSTRATIONS

Figure	Title	Page
1.	Effects of Reynolds Number, Roughness, and Rotation on Sphere Flow Pattern, Boundary Layer, and Forces . . . . .	8
2.	Summary of Physical Effects on $C_D$ Versus $R_d$ Representation . .	9
3.	Effect of Relative Mass on Lateral Excursion . . . . .	18
4.	Characteristics in The Critical $R_d$ Range. . . . .	21
5.	$C_D$ Versus $R_d$ For Spheres in Water. . . . .	26
6.	$C_D$ Versus $R_d$ For Spheres in Water, RM Effect . . . . .	27
7.	$C_D$ Versus $R_d$ For Spheres in Air. . . . .	29
8.	$C_D$ Versus $R_d$ For Superpressure Balloons (Scoggins Data) . . . .	31
9.	Shapes Tested in Gymnasium . . . . .	33
10.	$C_D$ Versus $R_d$ (Linear Plot) For Spheres and Spheres With Stabilizing Devices in Free Air. . . . .	34

## TECHNICAL MEMORANDUM X-53089

### STUDY OF SPHERE MOTIONS AND BALLOON WIND SENSORS

#### SUMMARY

Balloons ascending in still air typically exhibit lateral movements which introduce errors when the balloons are tracked as sensors of wind motion. This report examines some of the fundamentals of the fluid flows and associated motions and net drag coefficients of free-moving spheres. The flows and motions depend directly on Reynolds number ( $R_d$ ) which determines the flow regime; depend on the relative mass of the sphere to the fluid it displaces ( $RM$ ) because, for a given  $R_d$ , the lower the  $RM$  values the greater the lateral motions and thus the larger the total wake size and drag; and also depend on the sphere rotational inertia and minute details of surface roughness, sphericity, and random orientation. Because of these complex interactions no unique drag coefficient ( $C_D$ ) vs  $R_d$  curve can be found for free-moving spheres. The separate effects of the main factors are described as they might affect an idealized  $C_D$  vs  $R_d$  curve for a perfectly smooth free-moving sphere of infinite  $RM$ .

Observations were made of the mean vertical velocity and the magnitude of the lateral motions as spherical balls and balloons ascended and descended through both water and air, covering wide ranges of  $R_d$  and  $RM$ . The results are in general agreement with the physical concepts developed, and the water experiments give results consistent with the tests in air. In the subcritical  $R_d$  regime, where the wake separation is laminar, the motion tends to be a fairly regular zigzag, or spiral, of wave length on the order of 12 times the diameter. The magnitude of the lateral motion is roughly related to the factor  $(1 + 2RM)^{-1}$ . In the supercritical  $R_d$  regime, where the wake separation is turbulent and the wake is smaller, the motion tends to be an irregular meandering spiral. In the critical range of  $R_d$  the shift from subcritical to supercritical (and vice versa) flows and drags is rather abrupt; if sufficiently abrupt, there is a hysteresis effect with increasing and decreasing Reynolds number, and two stable velocities exist.

Tests were also made in air with spheres to which skirts, vanes, and/or drag chutes were affixed in an effort to stabilize the motion.



It is concluded that balloon motion can be smooth enough for most needs for high resolution atmospheric wind data if spherical or semi-spherical balloons are used operating always in the subcritical range, or certain balloons are used with roughness elements or other attachments operating at even higher Reynolds numbers.

## SECTION I. INTRODUCTION

FPS-16 high resolution radar tracking of 2-meter diameter spherical superpressure balloons has been used to provide detailed wind information for investigations relating to the wind loads on launch vehicles and for meteorological studies. The data points on the wind soundings show little scatter above approximately 11 km, but a great deal of scatter at lower altitudes. The scatter can be attributed to spurious lateral motions of the balloons, motions such as observed by Hirsch (1924), Bacon and Reid (1924), Killen (1960), and Henry and Scoggins (1963), and more recently by Scoggins (1964), Reid (1964), and Murrow and Henry (1964). For relatively large scale motions below 11 km and for even small scale motions above 11 km the balloon data are quite suitable (Stinson, et al., 1964), but a basic study of balloon motion characteristics was required (a) to define the validity of data at the low altitudes, and (b) to determine the optimum balloon configuration for the future which would be the best compromise between avoiding spurious motions, rising rapidly, having a short response distance, and being economical and easy to handle.

The mass of literature on sphere drag concentrates on the forces on spheres which are constrained in a wind tunnel or on an aircraft. Minor details of the mounting technique and tunnel turbulence are found to make large differences in the resulting forces, with the result that the direct extrapolation of these data to free-moving spheres is inappropriate. The literature on the detailed motion of free-moving spheres is not extensive; the references cited above and Lunnon (1925, 1928) represent major contributions.

The studies described here were initiated to provide a basic look at the balloon motion problem. At first, systematic trials were made in the atmosphere on ascending and descending spheres, and tests were conducted with various non-spherical shapes and drag devices. The atmospheric tests were inconvenient to perform and did not provide a wide range of size scales or a wide range of sphere densities. Therefore, a systematic series of tests was performed with small spheres in a swimming pool. Broad variations of the dominant parameters could be obtained readily with an assortment of toy balls. The sphere motions were easy to observe visually and photograph as the balls ascended or descended in the water. Although these tests were simple, they proved to be extremely illuminating and applicable to the atmospheric balloon case.

This report examines the underlying principles pertaining to the drags and motions of free-moving spheres, and then presents experimental data for motions in water and air. This must be considered as a preliminary report which is probing for the dominant factors. The data are not sufficiently complete to verify all the concepts, and the complexity of the numerous interrelationships means that precise answers will be difficult to obtain.

## SECTION II. DEFINITIONS AND RELATIONSHIPS

The motion of a balloon through the air is an example of the movement of a sphere through a fluid. It has proved convenient to discuss the factors in relation to the plot of drag coefficient ( $C_D$ ) vs Reynolds Number ( $R_d$ ). Drag coefficient is defined by

$$C_D = \frac{\text{drag}}{\frac{1}{2} \rho_f v^2 \pi \frac{d^2}{4}} = \frac{8 \times \text{drag}}{\pi \rho_f v^2 d^2} \quad (1)$$

where  $\rho_f$  is the fluid density,  $v$  is the mean vertical velocity, and  $d$  is the sphere diameter. The drag coefficient as used here is the effective drag coefficient taken from the averaged vertical component of velocity (the average vertical speed). When discussing the details of non-vertical motion, an alternative drag coefficient can be derived from the instantaneous vector speed, or equivalent lift coefficients established for the transverse motions, but these refinements will not be pursued here. The transverse motions of the sphere involve more energy being put into the fluid, and more fluid being affected, and hence the motions alter the total vertical drag and drag coefficient as defined in Equation (1).

The Reynolds Number is

$$R_d = \frac{v \cdot d}{\nu} \quad (2)$$

where  $\nu$  is the kinematic viscosity of the fluid ( $\nu = \text{viscosity}/\text{density}$ ). The  $R_d$  of a typical 2-meter diameter superpressure balloon will decrease from about  $1 \cdot 10^6$  at sea level to zero at the balloon's final equilibrium height. The balloon passes through many distinct flow regimes, regimes which fit into specific  $R_d$  ranges. The drag details are distinctly different in the different flow regimes. Thus the  $C_D$  vs.  $R_d$  plot is a basic form of data presentation, but it must be realized that effects of roughness, turbulence, and lateral motions will prevent the  $C_D$  vs  $R_d$  relationship from being unique.

For a given sphere and a given fluid density and  $\nu$ , velocity can be eliminated between Equations (1) and (2) and the equations combined as:

$$\log C_D = \text{Const.} - 2 \log R_d \quad (3)$$

Thus on a conventional log-log plot of  $C_D$  vs  $R_d$ , all points for a given sphere in a given fluid must lie along a specific line with a -2 slope. The points will vary along the line depending on the details of motion of the sphere.

The apparent mass of a sphere represents the mass of fluid which, in sphere acceleration calculations, can be considered as acting with the sphere. The apparent mass of a sphere in a perfect fluid turns out to be 1/2 of the mass of the displaced fluid. If the average density of a sphere is  $\rho_s$ , its mass is  $\rho_s \pi d^3/6$  and its total effective mass, real plus apparent, is  $\pi d^3(\rho_s + \rho_f/2)/6$ .

The relative mass, RM, of the sphere is the ratio of its mass to the mass of the displaced fluid. Thus  $RM = \rho_s/\rho_f$ . When the fluid is water RM is identical to the average specific gravity of the sphere.

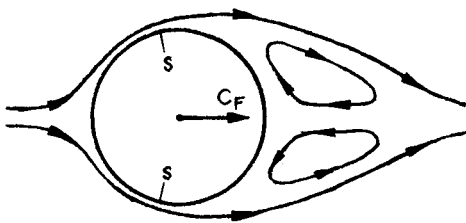
### SECTION III. FORCES AND FLUID MOTIONS FOR FIXED AND FREELY MOVING SPHERES.

Attempts to discover and understand the detailed nature of flow around a sphere span four centuries, beginning with the descriptive sketches of Leonardo da Vinci and the calculations of Newton, who also performed accurate tests on glass and hog-bladder spheres dropped from the dome of St. Paul's Cathedral. However, this deceptively simple shape involves extremely complex aerodynamic phenomena which still remain somewhat enigmatic to both experimental aerodynamicists and theoreticians.

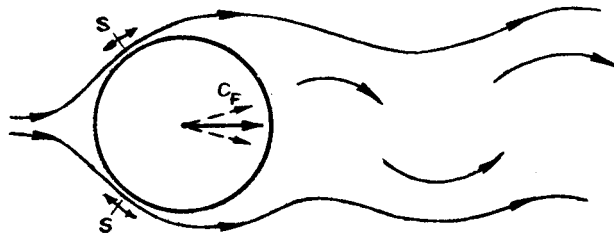
Figures 1 and 2 present sketches illustrating the sphere-flow phenomena which play a dominant role in establishing the fluid flow and motion of a free-moving sphere. Some of the details are based on conjecture, but in general the features are consistent with experimental data and involve logical physical principles. Figure 1 indicates the flow patterns, based essentially on classical wind tunnel measurements, with the sphere rigidly fixed. Figure 2 gives  $C_D$  vs  $R_d$  plots, extending the concepts to free-moving unsupported spheres.

The most influential similarity parameter relating the variety of flow patterns is the Reynolds number,  $R_d$ , the ratio of fluid inertial forces to viscous forces. At very low Reynolds numbers, the viscous shear forces in the boundary layer (BL) of fluid near the surface predominate over the pressure-inducing inertial forces, and smooth flow patterns result. As  $R_d$  is increased the viscous forces are no longer sufficient to damp any inertial oscillations in the boundary layer, and transition from a laminar BL to a turbulent BL occurs as the oscillations break up into tiny swirls. The physical nature of transition can be easily observed in the ascending smoke column from a cigarette in still air, where the sensitivity of the transition point (T) to flow disturbances is also clearly apparent. Separation occurs when the boundary layer can no longer negotiate the curvature required for the external flow to follow the body contour, and a wake or "deadwater" region results behind the body. The separation point (S) moves aft for the thin, energetic turbulent BL at very high  $R_d$ , moves forward for the thicker turbulent BL at lower  $R_d$ , and actually turns out to be on the forward hemisphere at low  $R_d$  with entirely laminar BL. From pressure effects a larger wake causes a larger drag coefficient, and so  $C_D$  is very sensitive to  $R_d$  via the strong influence of  $R_d$  on the boundary layer and wake flow patterns. Thus for spheres,  $R_d$  is the

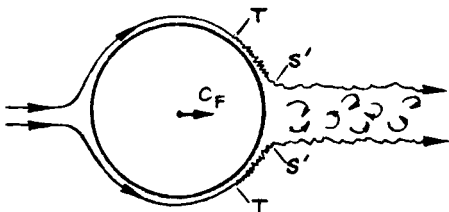
S = Separation T = Transition R = Rotation



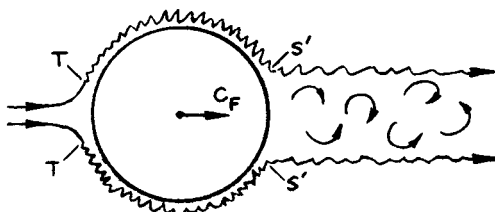
A.  $R_d \approx 1,000$  to  $10,000$   
Laminar BL; Closed wake  
 $\overline{C_D} \approx .4$ ,  $\overline{C_L} = 0$



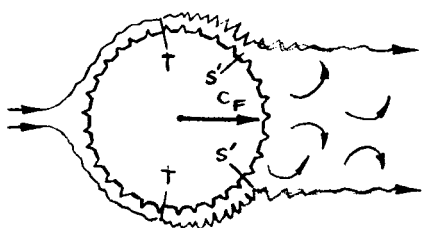
B.  $R_d \approx 10,000$  to  $200,000$   
Subcritical BL; Laminar separation  
 $\overline{C_D} \approx .5$  to  $1.0$ ,  $\overline{C_L} \approx \pm .1$  to  $.2$



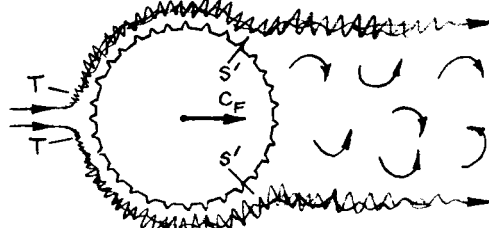
C.  $R_d \approx 400,000$   
Just-supercritical BL; Turbulent separation  
 $\overline{C_D} \approx .27$ ,  $\overline{C_L} = 0$



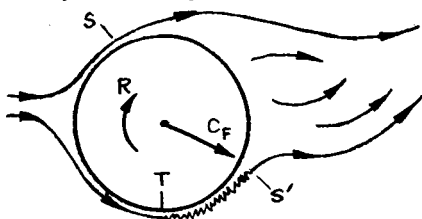
D.  $R_d = \text{Greater than } 1,000,000$   
Completely turbulent BL; Turbulent separation  
 $C_D \approx .3$ ,  $C_L = 0$



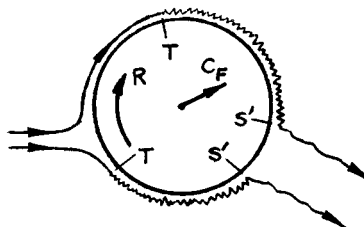
E. Effect of small roughness  
 $R_d \approx 200,000$   
 $C_D \approx .4+$ ,  $C_L = 0$



F. Effect of small roughness  
 $R_d \gg \text{Supercritical}$   
 $C_D \approx .3+$ ,  $C_L = 0$

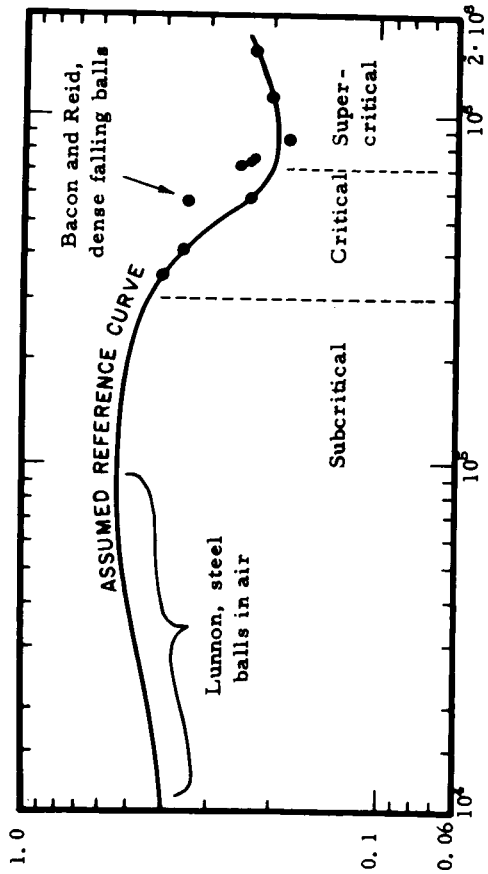


G. Effect of rotation  
 $R_d = \text{Subcritical}$   
 $C_D \approx 1.0+$ ,  $C_L \approx -.2+$

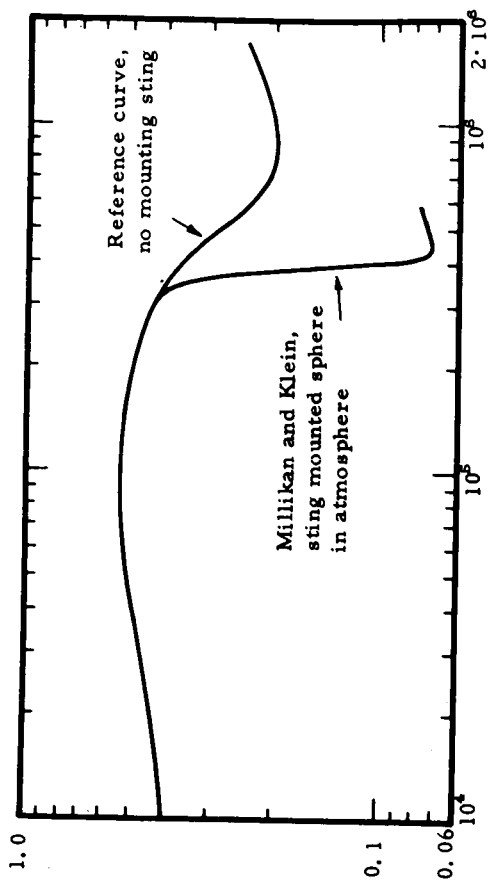


H. Effect of rotation  
 $R_d = \text{Supercritical}$   
 $C_D \approx .2$ ,  $C_L \approx .05$

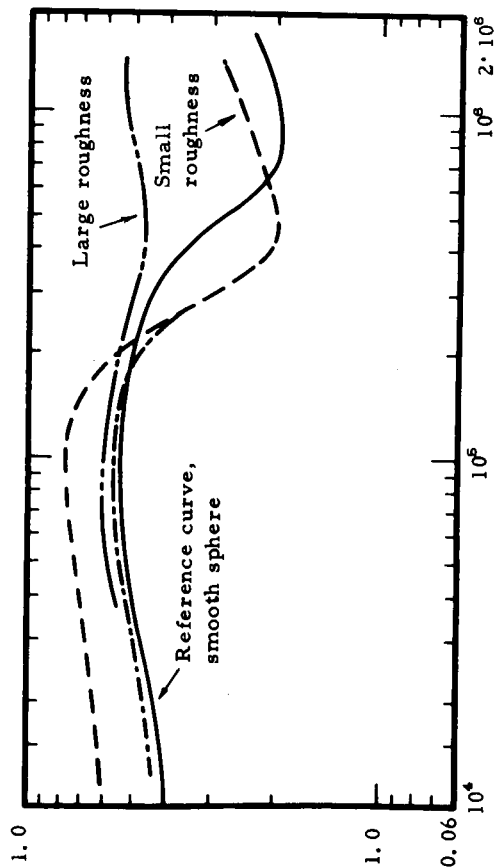
FIGURE 1. EFFECTS OF REYNOLDS NUMBER, ROUGHNESS, AND ROTATION ON SPHERE FLOW PATTERN, BOUNDARY LAYER, AND FORCES



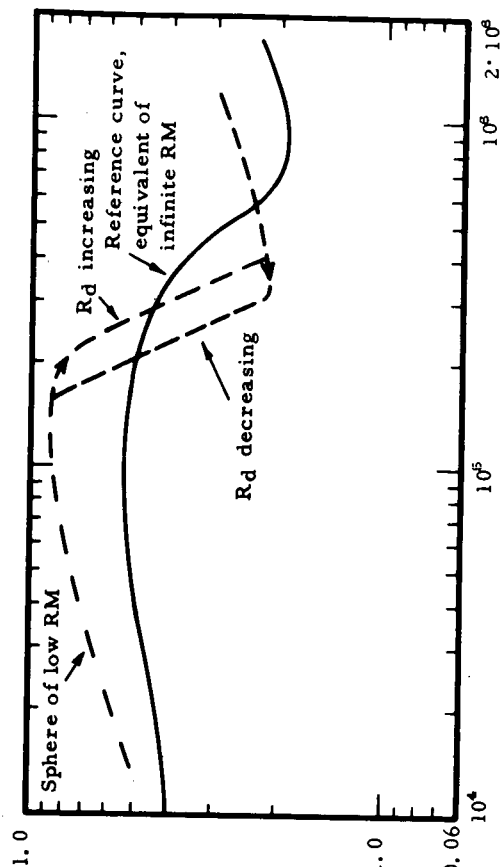
A. Reference curve for spheres of very high relative mass.



B. Effect of a sting mount on drag.



C. Effect of roughness on drag.



D. Effect of low relative mass (permitting lateral motion).

FIGURE 2. SUMMARY OF PHYSICAL EFFECTS ON  $C_D$  VERSUS  $R_d$  REPRESENTATION



dominant parameter affecting  $C_D$ , and  $C_D$  is usually plotted vs  $R_d$  on log-log scales to cover properly the wide range of  $R_d$  experienced in typical applications.

Consider the specific effect of  $R_d$  on the flow patterns and forces for a rigid sphere, as shown in Figure 1A - 1D. Note that the resultant force from the lift and drag components is represented by the force coefficient,  $C_F$  ( $C_F^2 = C_L^2 + C_D^2$ ), with  $C_L$  and  $C_D$  the lift and drag coefficients, respectively.

Stokes Regime,  $R_d < 1.0$  (not shown) There is no separation or wake but the BL is thicker than the diameter.  $C_D$  is very high ( $>10.0$ ) and falls off as  $1/R_d$ .

Very low Reynolds number,  $1 < R_d < 1000$ , (not shown) This is a transition region in which the BL shrinks and a wake starts to appear.  $C_D$  is decreasing with  $1/R_d$ .

Low Reynolds number,  $R_d \doteq 1000$  to  $10,000$  (Figure 1-A) The thick laminar BL separates on the front hemisphere, (at S) but the wake is closed and stable.  $C_D$  is at its lowest level for laminar BL conditions and there are no lifting forces.

Subcritical Regime,  $R_d \doteq 10,000$  to  $200,000$  (Figure 1-B) The thin laminar BL separates on the front hemisphere, the wake is very unsteady, and it leaves in oscillating or spiral flow patterns.  $C_D$  is high and fairly constant with  $R_d$ . The unsteady wake causes the separation points to vary with time and the resultant force to oscillate or spiral at a  $10^\circ$ - $20^\circ$  angle, even for rigidly constrained spheres.

Critical Regime,  $R_d \doteq 200,000$  to  $400,000$  (Figure 1-C) The critical regime occurs between the distinctly laminar separation and distinctly turbulent separation situations. Transition of the BL from the laminar to the turbulent type (at T) permits the BL to remain attached nearly all the way around the sphere, and  $C_D$  drops suddenly as the wake is reduced and stabilized. The exact  $R_d$  range of the critical regime and the steepness of the drop in  $C_D$  vs  $R_d$  depend on other influences (such as rigidity of restraint, the type of mounting sting, smoothness of the surface, air turbulence, and rotation of the sphere) and so will show large

differences for different cases. In the critical  $R_d$  regimes the net force is much steadier than in the subcritical, at least for a sting mounted sphere in a wind tunnel.

Supercritical Regime,  $R_d \dot{=} 400,000$  to  $100,000,000$  (Figure 1-D)

Transition moves up toward the front of the sphere as  $R_d$  increases, and the thickening turbulent BL separates somewhat more easily than the previous case.  $C_D$  is increased slightly with  $R_d$  due to increased friction of the turbulent BL and the larger separated region. The turbulent wake tends to give a steady force coefficient for a sting-mounted sphere. For balloons, without the stabilizing sting, minute surface variations can result in significant variations in the separation points and hence in wake position and side forces.

Very high Reynolds numbers,  $R_d > 100,000,000$  (not shown) The BL becomes negligibly small and the flow approaches ideal fluid flow without any separation.  $C_D$  gradually decreases with  $R_d$  to levels below 0.10 and is due mostly to the decreasing skin friction coefficient. This situation is simulated by large sting-supported wind-tunnel spheres at lower  $R_d$ , where the sting acts to stabilize the wake and reduce the separation region, but it can seldom be achieved in free air due to the exceptionally smooth and perfect surface required.

A second important influence on the flow pattern is sphere roughness. Figure 1-E shows how moderately small roughness (on the order of 1 per cent of the diameter) can cause BL transition to occur at subcritical  $R_d$ , thus reducing  $C_D$  by preventing laminar separation and moving the apparent critical region to lower  $R_d$ . At supercritical  $R_d$  (Figure 1-F)  $C_D$  is higher than that for natural transition on a smooth sphere (Case 1-C) because of the higher skin friction and because of the larger wake due to earlier turbulent separation at  $S'$  resulting from the thicker turbulent boundary layer. Large roughness elements (on the order of several per cent of  $d$ ) can even out the ratio of sub- to supercritical  $C_D$  by forcing such a thick turbulent BL that extensive turbulent separation occurs over both ranges of  $R_d$ . The consequently large wake drag masks the increase in friction drag. For intermediate roughness there is a race between the friction and wake drags, as  $R_d$  increases, which may leave a distinct dip between the sub- and supercritical drag coefficient levels.

A third important influence on sphere flow and forces is the sphere rotation. Rolling about the velocity vector stabilizes any spiral wake tendencies and thus may reduce  $C_D$  somewhat in the subcritical and supercritical ranges of  $R_d$ . Pitching or yawing about axes perpendicular to the velocity vector produce much more serious effects, as shown in Figure 1G and 1H. For the same nose-up pitching rotation shown in each case, a negative lift force occurs at subcritical  $R_d$ , but a positive lift occurs at supercritical  $R_d$ . These "Magnus forces," as they are called, result from the asymmetric separation induced by rotation effects. At subcritical  $R_d$ , the rotation causes premature separation on the downwind side and transition on the upwind side, thus deflecting the wake upward and yielding a downward lift force. At supercritical  $R_d$ , the boundary layer is dragged around with the sphere and circulation is induced, separation occurs on the bottom side, and a positive lift force results.

Since the factors determining the flow and motion are so numerous and are interrelated in a complex fashion, no simple  $C_D$  vs  $R_d$  curve for free-moving spheres can be universally valid. It is convenient to try to start with an idealized  $C_D$  vs  $R_d$  representation, and then show how and why various factors alter the curve, as shown in Figure 2. Figure 2A suggests the idealized reference curve. This is considered to represent  $C_D$  vs  $R_d$  for a perfectly smooth, perfectly spherical, non-rotating sphere, moving uniformly in non-turbulent air. The uniform movement requires, in effect, that the sphere has infinite mass relative to the surrounding fluid and thus does not accelerate, or, conceptually, that it is held fixed in a perfect wind tunnel by some non-mechanical means (say magnetically) so that no wires or sting support is involved. The particular shape of this  $C_D$  vs  $R_d$  reference curve is derived from fitting it to the data of Lunnon (1925) and Bacon and Reid (1924), who made measurements on the fall through air of dense spheres which had very high RM values and assertedly negligible lateral motions.

Figure 2A shows the two distinct  $R_d$  regimes: the subcritical, here  $R_d < 300,000$  where the drag is high because of the large wake resulting from laminar separation, and the supercritical, here  $R_d > 700,000$  where the drag is low since the wake is left small by the greater resistance to separation of the boundary layer. The critical  $R_d$  regime between these has a relatively rapid change of  $C_D$  with  $R_d$ . In the supercritical regime,  $C_D$  increases as  $R_d$  increases

because a larger and larger portion of the boundary layer is becoming turbulent, and the wake is increasing slightly due to increased turbulent separation. This effect accounts for the minimum in the  $C_D$  vs  $R_d$  curve just above critical  $R_d$ .

Figure 2B shows the effect of a sting or spindle mounting on the drag coefficient. The sting, entering the sphere from the rear parallel to the mean flow, tends to stabilize the spiral wake and both decrease  $C_D$  and extend the supercritical regime to much lower  $R_d$ . The effect is small with the big wake in the subcritical regime. The critical  $R_d$  regime is made smaller and the  $C_D$  variation with  $R_d$  is very abrupt (Hoerner, 1935). The effect of a particular sting or wire support is difficult to establish accurately because the effect depends somewhat on the turbulence and the mount vibration, factors which are appreciable in any tunnel tests and even in the Millikan and Klein (1933) data used on Figure 2B. Bacon and Reid (1924) and Hoerner (1935) provide a good review of the effects of stings and the difficulty of obtaining compatible results from different tunnels and different test setups.

The qualitative effects of sphere surface roughness are shown in Figure 2C. The skin friction portion of the drag is increased at both sub- and supercritical conditions, but this increase may be masked by larger changes in separation drag, depending on the degree of roughness. Small roughness acts primarily to trigger transition at lower  $R_d$  and thus gives a  $C_D$  vs  $R_d$  which is shifted to lower  $R_d$ . Very large roughness increases the turbulent separation at large  $R_d$  so much that  $C_D$  is near subcritical value (for smooth spheres), while at  $R_d$  large roughness will stabilize and reduce the wake and give  $C_D$  comparable to, or even less than, rigidly mounted spheres having laminar separation. The exact shape of  $C_D$  vs  $R_d$  in such cases depends on the details of the roughness and cannot easily be generalized.

Fine-grain fluid turbulence often encountered in wind-tunnels or similar test facilities has an effect on  $C_D$  vs  $R_d$  similar to that of roughness (Hoerner, 1935). Atmospheric turbulence at altitudes well above the ground does not contain much energy in the small eddy sizes which would have an appreciable effect on the balloon boundary layer configuration, and so should be a relatively minor influence. However, the ascent data on superpressure balloons at high altitudes suggest that occasionally, when  $R_d$  has just lowered to a subcritical value,

the balloon enters a turbulent area and for a short time shows characteristics of the supercritical regime (low  $C_D$  and fast rise, and more erratic data). The erratic data might merely be the result of the turbulence, but the fact that the vertical velocity always rises in these cases suggests that the phenomenon does pertain to the balloon temporarily switching back to the supercritical regime.

Figure 2D outlines the effect of permitting the balloon to have lateral motions which couple with the wake flow. The sphere thus affects a larger amount of fluid and has higher drag. The sphere moves faster than its mean vertical velocity  $v$ , and so even if locally it had the reference  $C_D$  vs  $R_d$  curve, when average values are used the curve would end up displaced upward because the apparent  $C_D$  is increased, and displaced to the left because the apparent  $R_d$  is lowered. The local  $C_D$  is actually greater than the reference curve value, one reason being that the mass and apparent mass require extra energy to accelerate the sphere around.

The free-to-move  $C_D$  vs  $R_d$  curve is steeper in the critical regime. One can think of this as being somewhat analogous to the sting mount effect of Figure 2B. In the free-moving sphere case the sphere motion tends to couple to the wake, somewhat stabilizing the wake with respect to the sphere. Because the  $C_D$  vs  $R_d$  curve may have a slope exceeding -2 on this log-log diagram, there can be a 2-valued hysteresis effect, depending on whether  $R_d$  is increasing or decreasing, accompanied by a sharp jump in  $C_D$  and  $R_d$  along the curve. These effects are discussed in detail later.

At subcritical  $R_d$  the motions tend to be somewhat regular zigzags or spirals, with a wave length on the order of  $12 d$ . The magnitude of the lateral motions in the subcritical  $R_d$  is shown later to be related, very approximately, to the factor  $(1 + 2RM)^{-1}$ . At supercritical  $R_d$  the motion is more random meandering because minute surface details and sphere orientation can trip the turbulent separation at different points and direct the small wake in a very different direction. Examples of superpressure balloon motions in the subcritical and supercritical regimes are given by Henry and Scoggins (1963), Scoggins (1964), Stinson, Weinstein, and Reiter (1964), Murrow and Henry (1964), and Reid (1964).

Figure 2 has illustrated some of the dominant effects. Many other details should be considered if the picture is to be complete. For example, the gross motions of a balloon often couple with rotation of the balloon (such as rocking of the sphere in zigzag motion, about

an axis perpendicular to the plane of the zigzag, or rotation around a vertical axis in spiraling motion, or pitching during meandering). Thus the moment of inertia of the balloon can be of importance, as well as small irregularities, surface features, and the random orientation of the balloon. It would be desirable to relate  $C_D$  to some unique function of  $R_d$ ,  $RM$ , inertia, roughness, and perhaps smaller effects, but it appears that the complete relation would be impossibly complex. Thus it seems most fruitful in this preliminary study to consider  $C_D$  vs  $R_d$ , and treat the other variables and the motions descriptively.

#### SECTION IV. THE RELATIVE MASS EFFECT

A dense sphere should logically exhibit less transverse motion and have a lower average drag coefficient than a non-dense sphere, if both are operating near the same  $R_d$ . Thus a light ball ascending through water should move side-to-side more than if the same ball were weighted to descend at a comparable speed (and thus comparable  $R_d$ ) through the water. This effect is considered as relating to RM. For a given disturbing force the lateral accelerations depend on total effective mass (sphere mass plus apparent mass) rather than only on the sphere mass, and so, for RM values considerably less than 0.5, the motion magnitude should not depend particularly on the exact RM value.

The details of the RM effect on the lateral motions of spheres and on  $C_D$  are exceedingly complex. Nevertheless, it is instructive to try to make an order-of-magnitude estimate based on simple physical grounds to reveal the relationships among parameters, at least for the common type of cyclic motion observed. A measure of the motion magnitude is the ratio of sideward to average vertical velocity,  $v_t/v$ , or the corresponding maximum deviation angle  $y_{\max}/(\lambda/2)$ , or the corresponding average deviation angle  $\bar{y}$  as the "motion magnitude" factor. The experiments suggested that in the simplest case of a zigzag path an impulsive transverse lift force (possibly due to vortex shedding) was applied in opposite directions every 3 to 10 diameters of sphere travel. The change in transverse velocity is due to the lift impulse  $I_L$  which acts for a short time  $\Delta t_i$ , corresponding to a short distance of travel  $\Delta x$ .

$$\Delta x = n d \quad (4)$$

where  $n$  is thus the number of diameters over which the impulse acts ( $n$  is of order unity). Let  $\Delta v_t$  be the velocity change between when the sphere is moving to the right and when it is moving to the left ( $\Delta v_t = 2v_t$ )

$$\Delta v_t = I_L / m_e \quad (5)$$

where

$$I_L = L \Delta t_i = C_{LI} \left( \frac{\rho_f}{2} v^2 \right) \left( \frac{\pi d^2}{4} \right) \left( \frac{\Delta x}{v} \right) \quad (6)$$

and

$$m_e = \pi d^3 (\rho_s + \rho_f / 2) / 6, \text{ effective mass} \quad (7)$$

The average zigzag angle (actually the tangent of the angle) is given by

$$\bar{\gamma} = \frac{y_{\max}}{(\lambda/2)} \quad (8)$$

For zigzags with very sharp corners,  $\bar{\gamma}$  can be approximated by the average velocities:

$$\bar{\gamma} \doteq \frac{vt}{v} \quad (9)$$

Substituting Equations (4) through (7) and the definition  $RM = \rho_s/\rho_f$  into Equation (9):

$$\bar{\gamma} = \frac{3}{4} \frac{C_{LI} n}{(2RM + 1)} \quad (10)$$

Experimental data from some of the swimming pool tests showing lateral angle vs  $RM$  are shown in Figure 3. Equation (10) is also plotted on Figure 3 with  $C_{LI} n = 0.5$  (say  $n = 1.0$  and  $C_{LI} \doteq 0.5$ ). These values of  $n$  and  $C_{LI}$  give some agreement with the zigzag data points and are not unreasonable from an aerodynamic standpoint. The derivation is made for a zigzag trajectory, not for the stable spiral motions sometimes encountered in the subcritical regime. Figure 3 includes data points pertaining to both cases.

The relations between  $RM$ , the side motions, and  $C_D$  will be considered later in the discussion of the experimental data. The main point of the analysis just presented is that the relative amount of lateral motion should depend on the factor  $(1 + 2RM)^{-1}$ . Thus the maximum effect will pertain to the lightest spheres, but the effect has a limit even for zero weight spheres because of the apparent mass term. The lateral motions can be expected to be very small as  $RM$  exceeds 100, as for ordinary solid rubber balls in air, but appreciable lateral motions will occur for beach balls and balloons in air.

An asymmetry in the position of the wake of the sphere can readily give a sideways force or lift coefficient on the order of 0.1. If this flow configuration lasts for a long time, the lateral excursion of the sphere can be quite large. In the above derivation of the "motion magnitude" factor it was assumed that the flow configuration altered significantly after the sphere moved vertically a fixed number of diameters. The distance to establish a significantly different flow regime could have been taken alternatively as the response distance, the distance traveled in unit time, or some combination of these with a "number-of-diameters" distance. However, the "number-of-diameters"



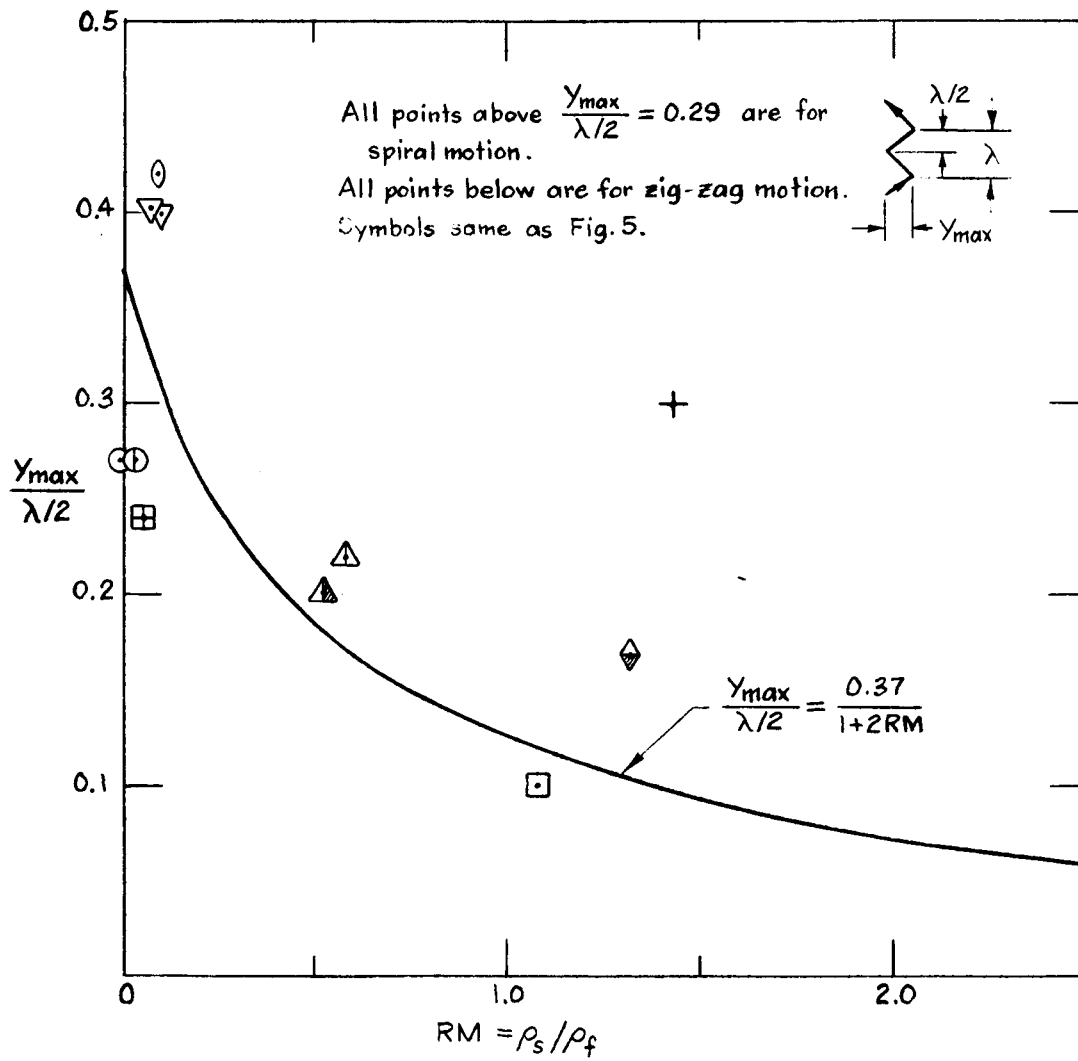


FIGURE 3. EFFECT OF RELATIVE MASS ON LATERAL EXCURSION

distance criterion alone seemed to be consistent with the experimental results as exemplified on Figure 3, and also seemed particularly logical on the basis of examination of the details of motion. A common form of motion was a true two-dimensional zigzag consisting of a straight ascent toward the other side, etc. It takes a flow of several diameters or chords for the flow regime to build up around any aerodynamic shape. When a balloon is released from rest it starts up vertically for a number of diameters and then rather abruptly manifests a sideways motion (seen regularly in the air and water tests reported here, and in the data of Hirsh (1924), Killen (1960), Henry and Scoggins (1963), and Murrow and Henry (1964)). A vortex is shed at the moment of abrupt flow change, and momentum is shifted in an impulsive effect. When the wake configuration and the sphere dynamics permit a stable spiral motion, the physical picture is somewhat different than the one discussed here; one of the data points for this spiral motion on Figure 3 shows more lateral motion than would fit the zigzag case. Nevertheless, the spiral and zigzag motions both represent rather regular motions with a distinct natural wave length (on the order of  $12d$  for the swimming pool tests of this report and for the superpressure balloon motions shown by Scoggins (1964)), and so qualitatively the effect of RM on lateral motion should be derivable by the type of analysis suggested above. For supercritical  $R_d$  where the motion becomes irregular meandering rather than a regular zigzag or spiral, the same sort of RM analysis cannot be expected to give applicable results. A particular lateral movement may last as long as the orientation of certain minute surface features remains the same relative to air flow, rather than changing after just a few diameters of ascent. The movement thus relates in a complex manner to the sphere surface configuration, its rotational inertia, its present orientation, and random effects. To the extent that the meanderings involve lateral accelerations, a high RM will still damp the lateral motions somewhat, but probably in a much weaker manner than for the spiral or zigzag cases.

Lunnon (1925) examined the fall of small metal spheres through air, with the result shown on Figure 2A. Lunnon (1928) observed the fall of metal spheres through liquids, including somewhat larger  $R_d$ , and found that the drag coefficients were about 25 per cent higher. He noted that "there is always some swerving in the path of falling spheres", and that swerving was just visible with a 1.27 cm diameter steel ball falling in water through 150 cm. It is possible that a partial cause of the larger drags he found in water arose because the RM was getting under 10.

## SECTION V. OPERATION IN THE CRITICAL RANGE OF REYNOLDS NUMBER

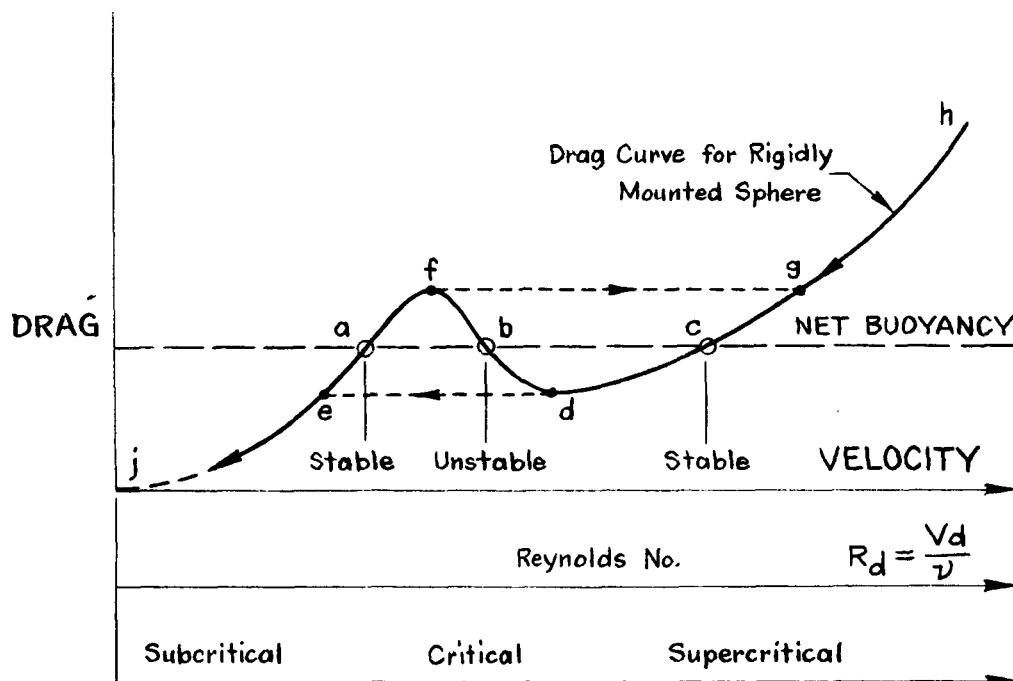
A freely ascending (buoyant) balloon or freely falling sphere has a constant apparent weight (positive or negative) which is opposed by the aerodynamic forces developed. A necessary but not sufficient condition for equilibrium velocity is that these forces balance each other. The sufficient condition is obtained when the equilibrium point is stable to small perturbations. Meeting the necessary and sufficient conditions precludes the measurement of the complete drag-coefficient versus Reynolds number curve in the region of critical Reynolds number for some free moving balloons. If a  $C_D$  vs  $R_d$  curve were measured by using very dense free moving spheres, a portion of the curve in the critical  $R_d$  range could not be observed if the actual  $C_D$  curve for this sphere showed a slope exceeding -2 on a log-log plot.

The critical range effect is most readily understood by considering a drag plot rather than a  $C_D$  plot. If one mounts a given sphere on a wind-tunnel force sensor, the plot of measured drag force versus velocity appears as in Figure 4-A.

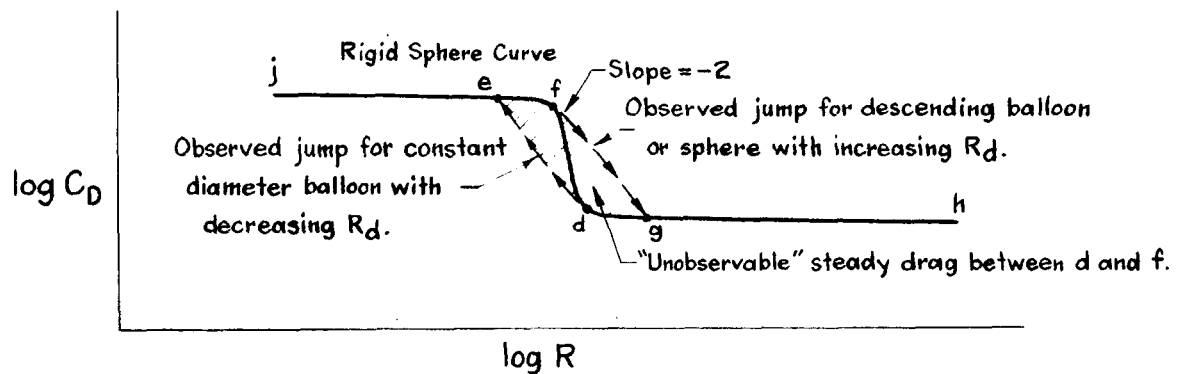
Now assume that a dense sphere is observed ascending through a fluid, that the sphere has drag characteristics similar to the tunnel measured data of Figure 4-A, and that the net buoyancy of the sphere can be altered as desired. In equilibrium, the drag of the sphere will equal the net buoyancy.

It is apparent that for the buoyancy shown by the dotted line, three potential equilibrium points exist at a, b, and c. However, only points a and c are stable against small disturbances in the velocity and thus only two stable ascent speeds are possible. At point b any perturbation in velocity or buoyancy would result in an imbalance between buoyancy and drag and the balloon would accelerate to point c or decelerate to point a. For buoyancy well below or above the critical levels only one equilibrium ascent speed is possible.

If the terminal velocity of an ascending sphere is plotted as the balloon ascends and  $R_d$  decreases, the drag-velocity curve will be h-g-c-d-e-j (at d the wake will be that associated with turbulent separation; then slightly less buoyancy will slow the sphere and the laminar separation regime will be established). Conversely, with weights added to a descending sphere so the  $R_d$  keeps increasing, the drag-velocity curve will



A. Sketch of Drag vs. Velocity or  $R_d$



B. Sketch of  $\log C_D$  vs.  $R_d$  Showing "Unobservable" Regime

FIGURE 4. CHARACTERISTICS IN THE CRITICAL  $R_d$  RANGE

be j-e-a-f-g-h. Thus the free-moving sphere data can never give equilibrium information as to the drag situation at  $R_d$  between f and d.

Figure 4A can be put into the form of the  $C_D$  vs  $R_d$  plot conventionally used for sphere drag presentations. This is done in Figure 4B. As has already been shown, for a given free moving sphere in a given fluid,

$$\log C_D = \text{Const} - 2 \log R_d$$

When plotted as a graph of  $C_D$  vs  $R_d$ , there is thus a discontinuity with a -2 slope between points d and e while decreasing  $R_d$  or f and g while increasing  $R_d$ .

Consider that the complete  $C_D$  vs  $R_d$  plot for a balloon can somehow be measured in a wind tunnel with the mean velocity of the sphere controlled as desired but the sphere still permitted to move about the mean position in order to duplicate free-fall conditions. If the slope of the  $\log C_D$  vs  $\log R_d$  curve is steeper than -2 in the critical  $R_d$  region, there will be an "unobservable" regime as shown in Figure 4B and the  $C_D$  vs  $R_d$  curves will differ in the critical  $R_d$  region for increasing  $R_d$  cases vs decreasing  $R_d$  cases. If the slope is not steeper than -2, as can presumably happen for certain cases of roughness and relative density, there will be no "unobservable" regime and the  $C_D$  vs  $R_d$  curve will be unique.

The jump from d to e for certain superpressure balloons ascending and having decreasing  $R_d$  regimes is apparent in data which will be presented later in this report; other data show some superpressure balloons do not have this "unobservable" regime. Tests at a single  $R_d$ , such as for the individual free movement cases in the swimming pool and gymnasium, must be interpreted as to whether they may fall in the subcritical or supercritical regime. Since the spheres are usually released at zero speed, one might assume that they reach equilibrium through an increasing  $R_d$  situation and so follow the e-f-g curve on Figure 4. In one set of rising sphere tests in the swimming pool (points shown on Figures 5 and 6) two distinct rise speeds were encountered in separate tests. Apparently in some cases the ascent would be subcritical, with low average velocity and the sphere not popping out of the surface. In other cases the ascent would be super-

critical, with fast velocity and the sphere actually exiting from the water. In the latter case, some slight variation in releasing the sphere at the pool bottom presumably permitted a momentary acceleration to supercritical motion. Because it takes a finite time to develop or adjust a wake to a new mean velocity situation, one often observes that spheres rising in water or air will accelerate quickly upon release, and then slow down after rising a short distance (Hirsch, 1924, Murrow and Henry, 1964, etc.). However, this unsteady flow-pattern effect should not be confused with the two-valued equilibrium velocity effect just described, which occurs for steady flow situations. Of course it is possible, and sometimes probable, especially if the  $C_D$  vs  $R_d$  plot has a slope very near -2, that operation in the critical regime results in coupling between the marginally stable flow patterns and the balloon's tendency to seek one of two ascent speeds, giving an erratic ascent velocity.

## SECTION VI. EXPERIMENTAL RESULTS AND INTERPRETATIONS

### A. The Experiments

In an attempt to clarify some of the concepts presented here, and provide clues concerning balloon motion which might help with the operational problems associated with the use of balloons as wind sensors, some experiments were conducted measuring the rise of balloons and beach balls in a large gymnasium, and the rise and fall of spheres in a swimming pool.

Tests were also conducted in the air with spheres having devices attached, and with non-spherical shapes. The water tests afforded the opportunity to cover conveniently a range of sphere roughnesses, masses, and  $R_d$  and  $R_M$ , and they served as the most effective experiments to illustrate the fundamentals of the flows and motions.

### B. Swimming Pool Tests

An assortment of spheres was procured, mostly toy balls, of diameters varying from 0.04 to 0.792 feet, and with  $R_M$  varying from 0.025 to 1.52. Certain of the hollow balls were filled with liquids to give them desired  $R_M$  values to vary the  $R_d$  of their motion as well as the  $R_M$ . All the spheres are listed in the table on Figure 5. The balls were selected for sphericity and regularity of surface. The styrofoam balls all had the typical styrofoam rough surface. All the other spheres were smooth-surfaced except for a small seam around the diameter; the seams were smoothed off with a razor blade. The "hole-ball" is a hollow plastic sphere perforated with large holes, selected by Reed and Lynch (1963) as a drag sphere to give wind measurements.

The spheres were released from a sieve on the end of a long pole, from just at the surface of the pool ( $R_M > 1$ ) or from the bottom at a depth of 9 feet ( $R_M < 1$ ). The details of the ascents and descents were observed visually, and recorded on color film with a movie camera pointing down vertically from about 7 feet above the pool, and with an underwater movie camera situated horizontally 23 feet from the spheres. Marking dots and grids were put on some of the spheres so rotations could be observed.

Average vertical velocities were determined by timing the spheres with a stopwatch during the visual observations (between the surface and the time the sphere passed the 6-foot depth level as ascertained with the aid of a 45° mirror set at that level), and by counting frames from the underwater camera (as the sphere moved between the surface and depth marks on a vertical marker stick set adjacent to the path of motion).

All the data deemed accurate are shown on Figure 5. The scatter of points such as for spheres #1, 4, 10, 12, 13, 20, and 26B on Figure 5 provides a general estimate of the over-all accuracy and reproducibility of these measurements. Points for a given sphere which show 2-valued scatter are assumed to demonstrate that somewhat different flow regimes were set up on consecutive trials. Note that for any given sphere, all the points lie on a line with a -2 slope, as mentioned in the discussion of Equation (3).

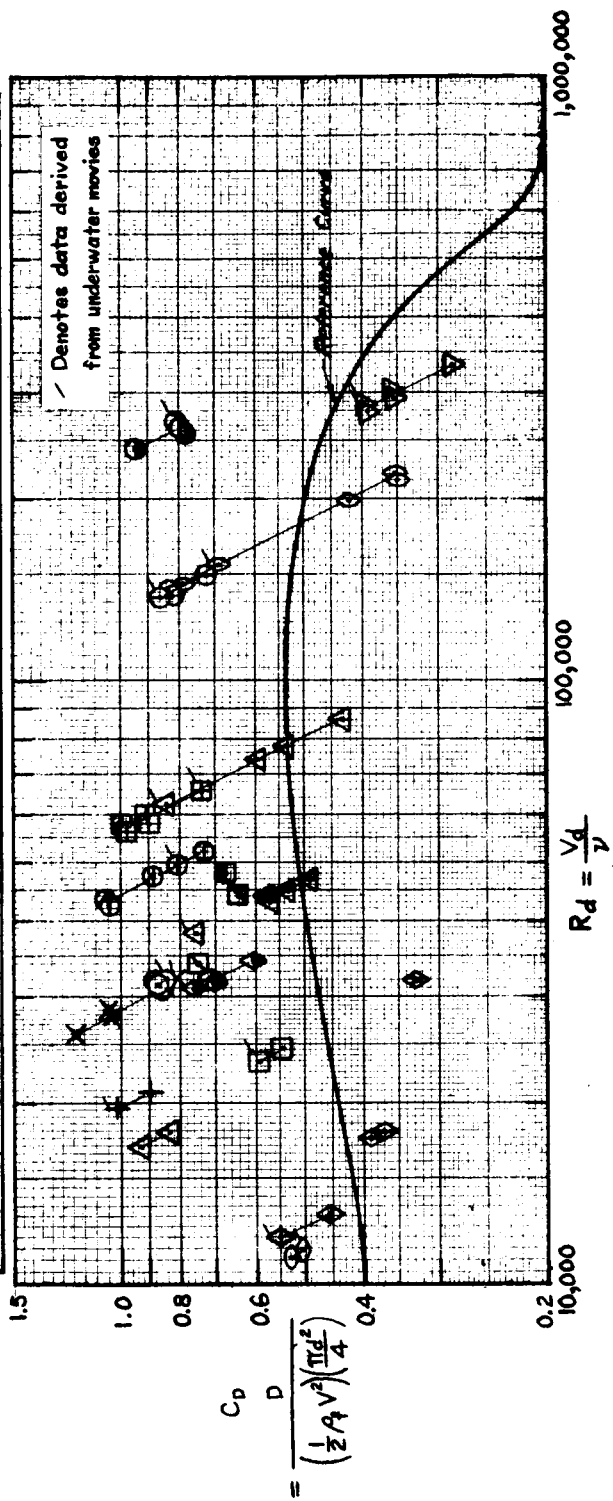
Sphere #22, large and very buoyant, operated at the highest  $R_d$  and was definitely in the supercritical regime. Its motion showed an irregular wandering spiral (to the extent that this could be observed within a 9-foot water depth). For reasons discussed earlier, Sphere #26A sometimes did not exit from the water, rising slowly in the subcritical regime, and sometimes did exit from the water, rising rapidly in the supercritical regime. Sphere #20 and all the other plotted points presumably represent motion in the subcritical regime.

As has previously been pointed out, no unique  $C_D$  vs  $R_d$  curve could be expected from spheres with varying roughness,  $d$ ,  $RM$ , and moment of inertia. The over-all scatter of points on Figure 5 is thus logical. To try to observe some stratification, Figure 6 was prepared, putting the data points of Figure 5 into three  $RM$  categories. As would be predicted from reasoning given earlier, for a narrow  $R_d$  range the lowest  $RM$  category is associated with the highest drag and  $C_D$  values.

The intermediate and high  $RM$  categories do not show any distinct  $C_D$  variations; however, this is perhaps not surprising because the "motion magnitude" factor  $(RM + 1)^{-1}$  only varies from 0.27 to 0.40 for the average  $RM$  in these respective categories (compared to 0.87 in the lowest  $RM$  category). It is possible that a slight effect of



SYMBOL	NO.	D (ft)	RM	TYPE	SYMBOL	NO.	D (ft)	RM	TYPE
□	1	.192	1.09	Teflon, F <sub>2</sub> (NO <sub>2</sub> ) <sub>2</sub> filled.	○	16	.121	.090	Styrofoam.
▤	2	.191	1.26	↓	⊖	17	.161	.096	
▥	3	.192	1.36		⊙	18	.235	.092	
▧	4	.191	.100	Teflon, empty.	⊖	19	.332	.092	
▩	5	.194	.100	↓	⊙	20	.494	.030	
▫	6	.194	1.52	Teflon, gravel filled.	▽	21	.792	.029	Rubber, air filled.
▬	7	.192	.100	Teflon, empty.		22	.412	.094	↓
▮	8	.062	1.22	Plastics, solid red.		23	.842	.025	Plastic, small bead.
◊	9	.063	1.27		+	24	.040	.952	Ping-pong ball, clay filled.
◈	10	.105	1.21			25	.112	1.43	Plastic, hollow black.
◉	11	.125	1.25		○	26	.333	.066	Plastic, partially H <sub>2</sub> O filled.
◊	12	.167	1.31		○	26A	.333	.112	Plastic, H <sub>2</sub> O filled.
◈	13	.113	.608		×	26B	.333	.96	Hole ball.
◊	14	.175	.993	Sponge rubber.		27	.345	.97-99	
◈	15	.240	.529			28	.122	.087	Ping-pong ball, red

FIGURE 5.  $C_D$  VERSUS  $R_d$  FOR SPHERES IN WATER

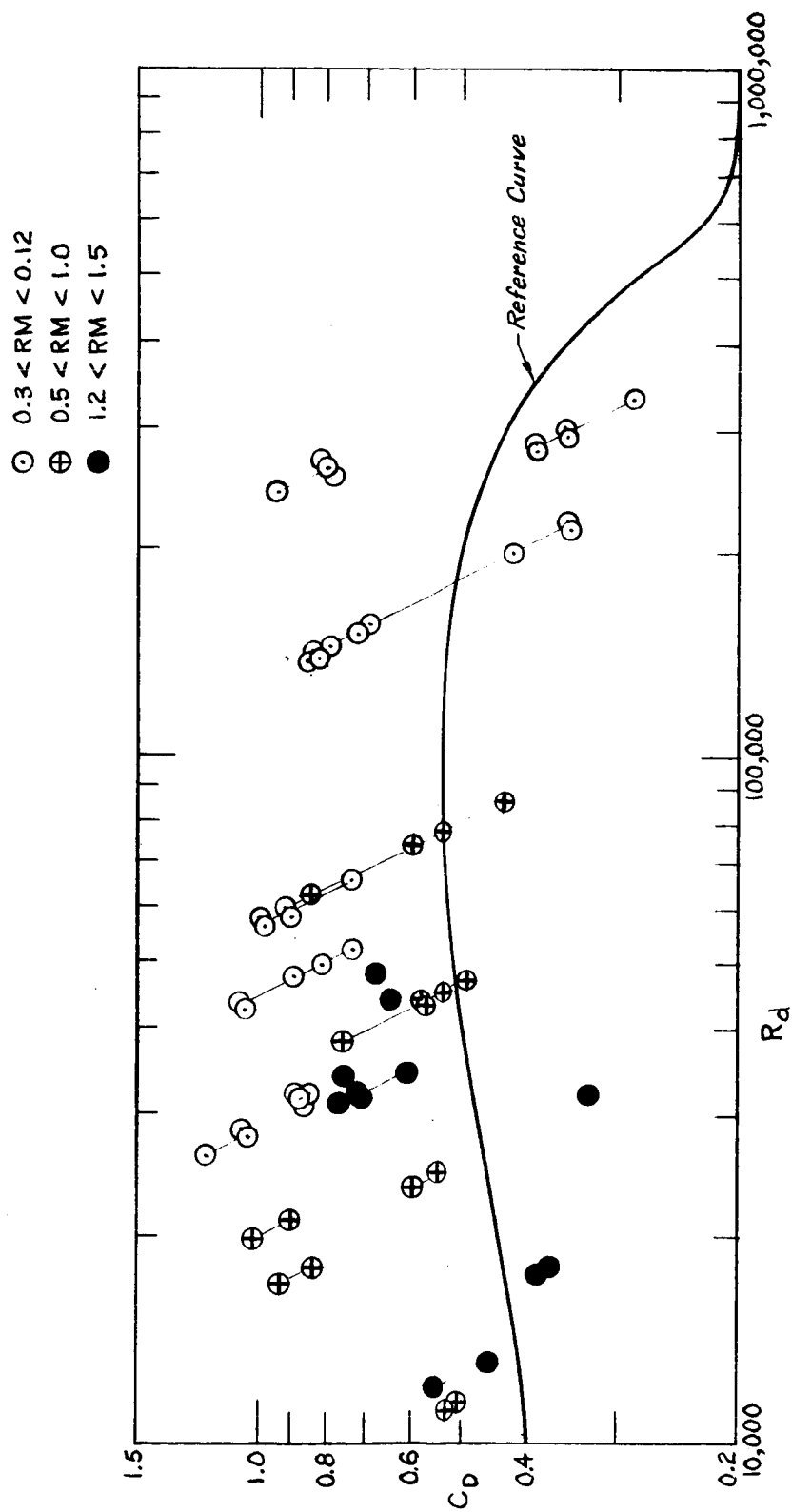


FIGURE 6.  $C_D$  VERSUS  $R_d$  FOR SPHERES IN WATER, RM EFFECT

roughness is hidden here; the roughest spheres, styrofoam also had the lowest RM.

Several other factors were shown by the pool tests. The very slow motion of the "hole-ball" and of another smooth sphere with  $RM \sim 0.98$  placed them at  $R_d$  values well below 10,000, and both exhibited perfectly straight ascents. These observations, together with observations of the motions of soap bubbles, suggest that lateral motions disappear at low  $R_d$ , and so it is hypothesized that if Figure 2D were extended down to  $R_d = 10^3$  the low RM dotted curve would merge with the  $RM = \infty$  reference curve.

Marbles were released at the surface, rolling out of the sieve with a decided spin. They would descend fairly straight but inclined at an angle of  $20^\circ$  or  $30^\circ$  to the surface, in the direction which would be expected from the Magnus forces of a conventional type (moving toward the downwind-traveling side of the pitching sphere).

Coupling between the lateral and rotational sphere motions was observed for many spheres. The most pronounced effect was a strong rocking which tied in exactly with the zigzag motions. (Ball No. 25)

In one case of a sphere spiraling up at subcritical  $R_d$  air bubbles were released at its base and showed that the wake motion was a perfect spiral following the path of movement. (Ball No. 26A)

In summary, at subcritical  $R_d$  the lateral motions were regular spirals or zigzags, while for the supercritical case the motions were more like wandering spirals.

### C. Spheres Ascending and Descending in Air

Tests were made with neoprene balloons ascending and beachballs descending in a gymnasium and with ascending neoprene balloons outside. Some of the ascent cases made use of a very light tether thread; it is believed this did not appreciably affect the data. The quantitative data were obtained by photogrammetry from movies from the side. Figure 7 presents the data.

In summary, the data are consistent with the RM concept sketched in the " $R_d$  increasing" curve of Figure 2D, but the data show considerable scatter. The beachball descents, with large RM,

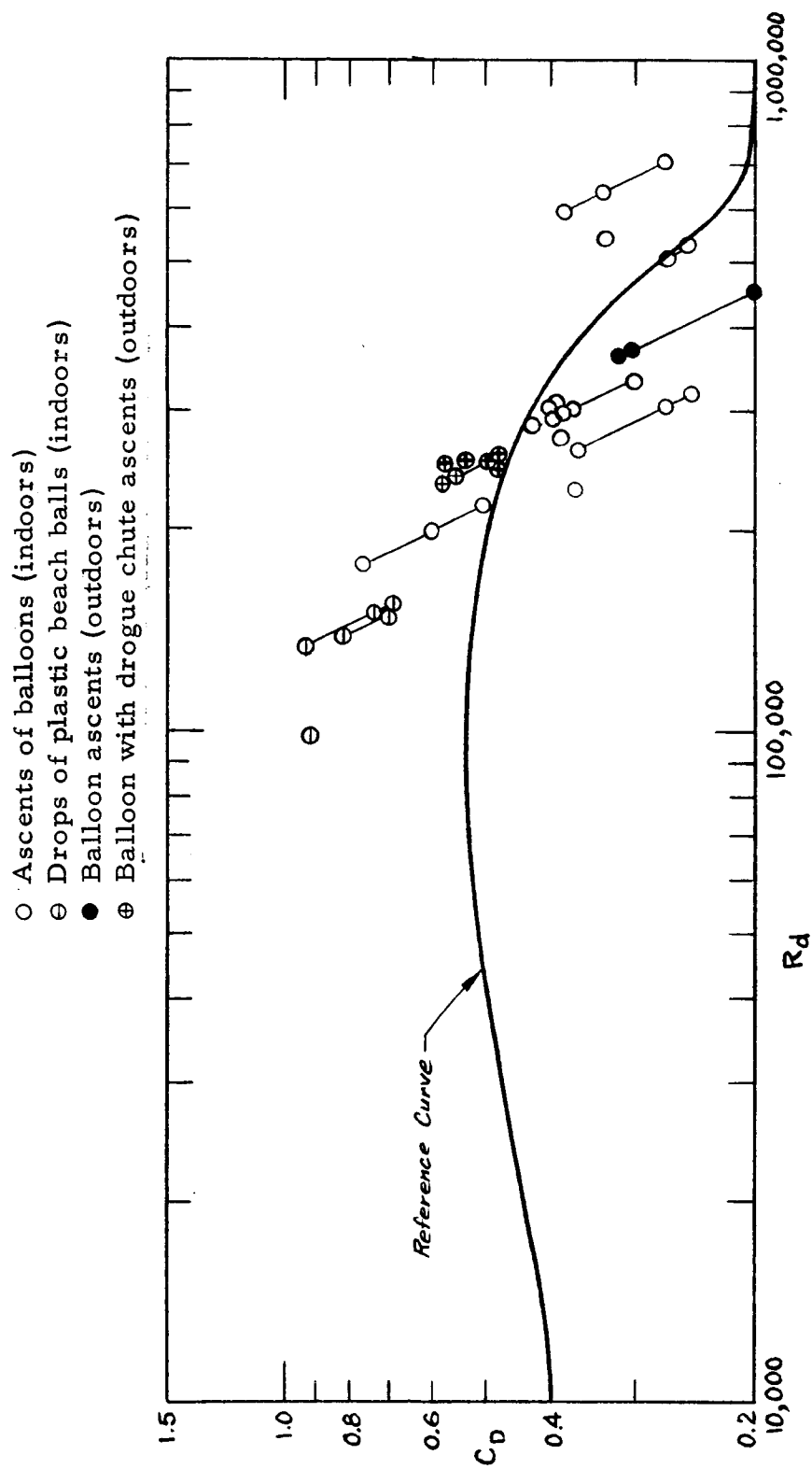


FIGURE 7.  $C_D$  VERSUS  $R_d$  FOR SPHERES IN AIR

all tend to be at low  $R_d$  and so cannot be directly compared to the low RM balloon ascents. In any case, both the ascents and descents at subcritical  $R_d$  are above the Reference Curve. The lineup of points for the rise of small neoprene balloons suggests that the data are showing the jump from subcritical to supercritical  $R_d$ , but that the jump is sometimes taking place part way along in the descent and so providing some points which are really not equilibrium points and which fill in the "jump, " Some of the supercritical regime points go well below the Reference Curve in agreement with Figure 2 D.

For the outdoor drogue chute cases, a light parachute was attached to the balloon to provide a vertical stabilization reference. The total lateral movements of the balloons were materially reduced; there was a higher frequency spiral motion of balloon and tail. The tails were put back at 8 to 10 diameters. It is possible that the  $C_D$  values represent subcritical motion with  $C_D$  reduced by the reduction of lateral motion.

#### D. Superpressure Balloon Data

Scoggins (NASA Aero-Astrodynamics Lab., Marshall Space Flight Center) has provided reduced data on the drag coefficients of several sizes of superpressure balloons which were tracked on March 18, 1963, by the FPS-16 as a comparison study. Figure 8 shows some of the results in the same format as the other curves presented here. Obviously spurious data points have been omitted. The curve for the 2-meter diameter balloon is taken from Scoggins (1964). The absolute values of  $C_D$  at the lowest  $R_d$  may be in error because of the difficulty in estimating buoyancy accurately at the peak altitudes. The data show a rather small amount of scatter, indicative of a lack of vertical turbulence in the air on this day, and suggesting how well relative vertical air velocities can be obtained from balloon data (the vertical velocity scatter is proportional to the square root of the  $C_D$  scatter).

All the curves of Figure 8 show the general sort of shape expected for lightweight spheres from Figure 2 D, but still there are distinct differences between the curves. The 2-meter diameter balloon curve has a slope never steeper than -2, and so there is no jump in the curve and none of the hysteresis effect shown in Figure 2 D and Figure 4. The 4-foot and 7-foot diameters do both show the jump, and so are following the " $R_d$  decreasing" portion of the Figure 2 D and Figure 4

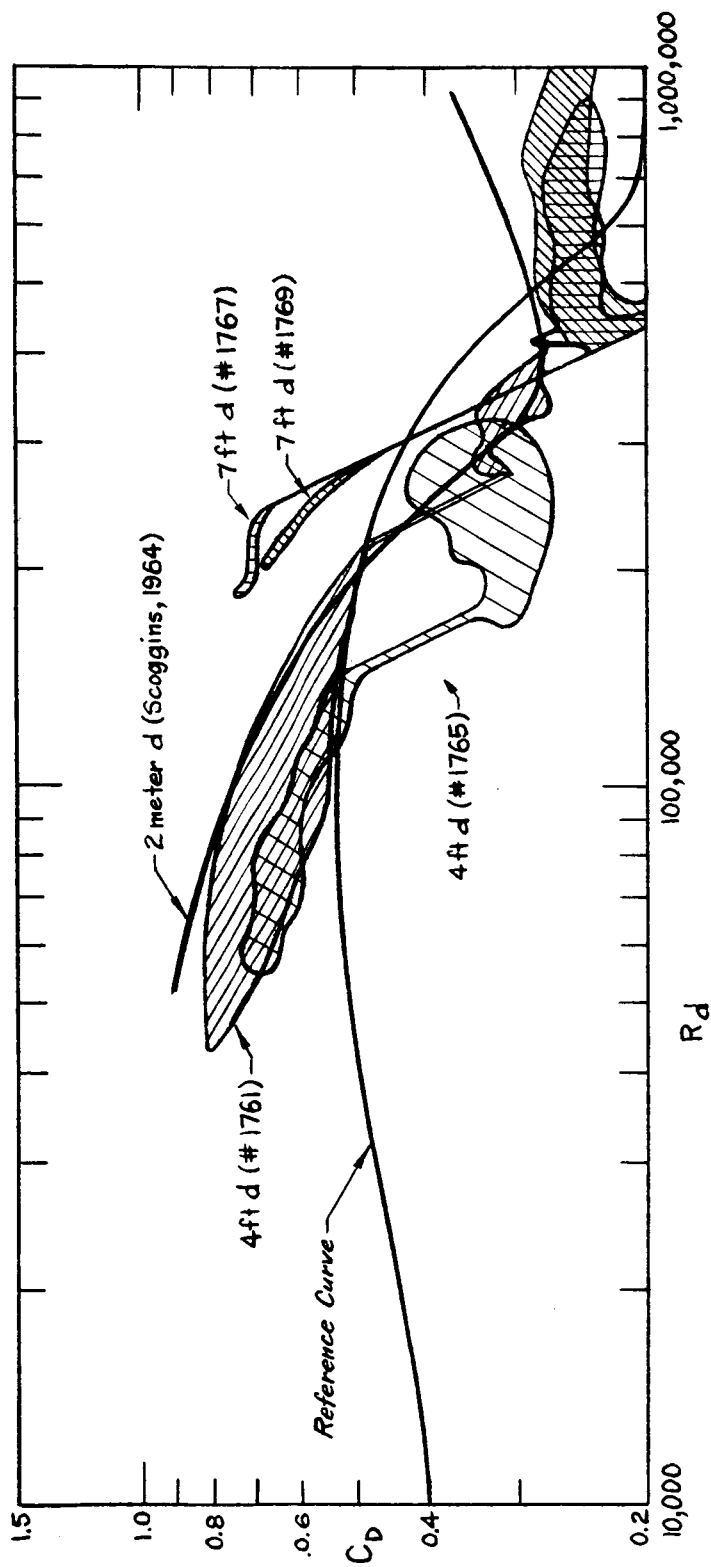


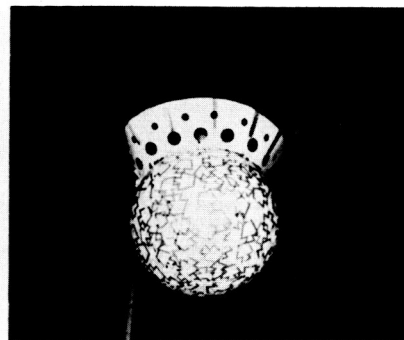
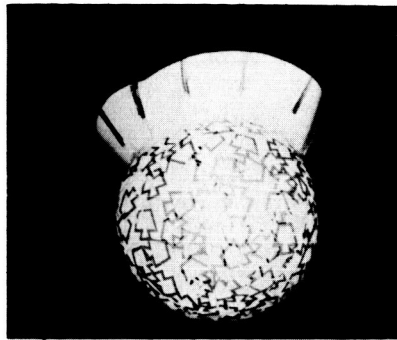
FIGURE 8.  $C_D$  VERSUS  $R_d$  FOR SUPERPRESSURE BALLOONS (Scoggins Data)

curves. It is presumed that the difference between curves on Figure 8 is a manifestation of the significant differences in flow and motion which can arise from the minute differences in individual balloon types. The size of the seams, the number of gores, and the configuration of the pressure relief valve can all have effects.

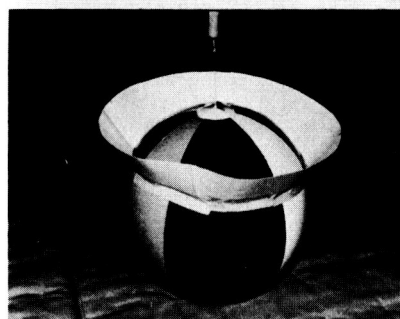
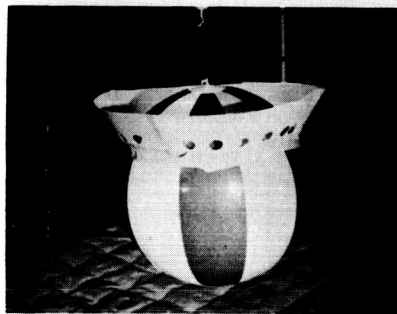
#### E. Non-Spherical Shapes

Figure 9 shows typical configurations which were tried in the gymnasium tests at the beginning of the program. All of the  $C_D$  vs  $R_d$  data for the gymnasium tests are presented in a linear plot on Figure 10, which therefore reproduces some of the data from Figure 7. The non-spherical cases shown on Figure 10, all of which are at  $R_d < 225,000$ , follow along with the spherical ones or else have slightly higher drag, with the expected low drag for the bomb-shaped units. The drops of the skirted devices showed the beginning of what appeared to be damped oscillations; the propeller fin device was more unstable; the bomb shape with canted fins gave a reasonable spiral motion.

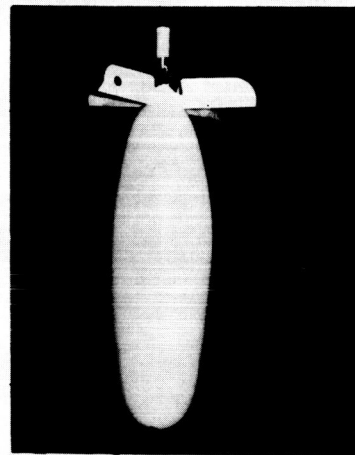
The optimum rigid tail configuration evolved in these tests was the "ventilated skirt" design (Figure 9 B, center), in which a truncated conical skirt having a base somewhat larger than the sphere diameter is provided with a ring of holes near the attachment to the sphere. The purpose of these holes is to ventilate the base to the nearly stagnation pressures in the windward side of the neck, while retaining the superior stabilizing forces near the edge of the solid skirt. However, even the best of these skirts will add appreciable weight to the basic balloon and thus reduce its terminal speed and altitude. Since all parts of a drogue chute operate in tension, a very light stabilizing device results and it emerges as the recommended solution.



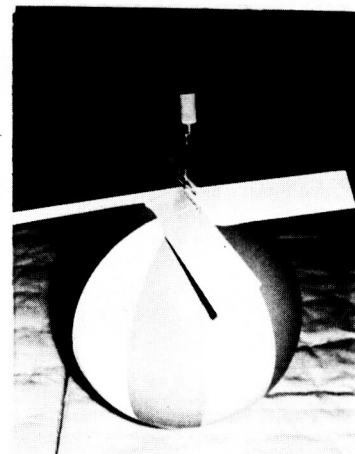
A. Small beach ball with solid and perforated aft skirt.



B. Large beach ball with perforated, ventilated, and solid aft skirts.



C. Bomb with shaped fins.



D. Large beach ball with propeller fins.

FIGURE 9. SHAPES TESTED IN GYMNASIUM



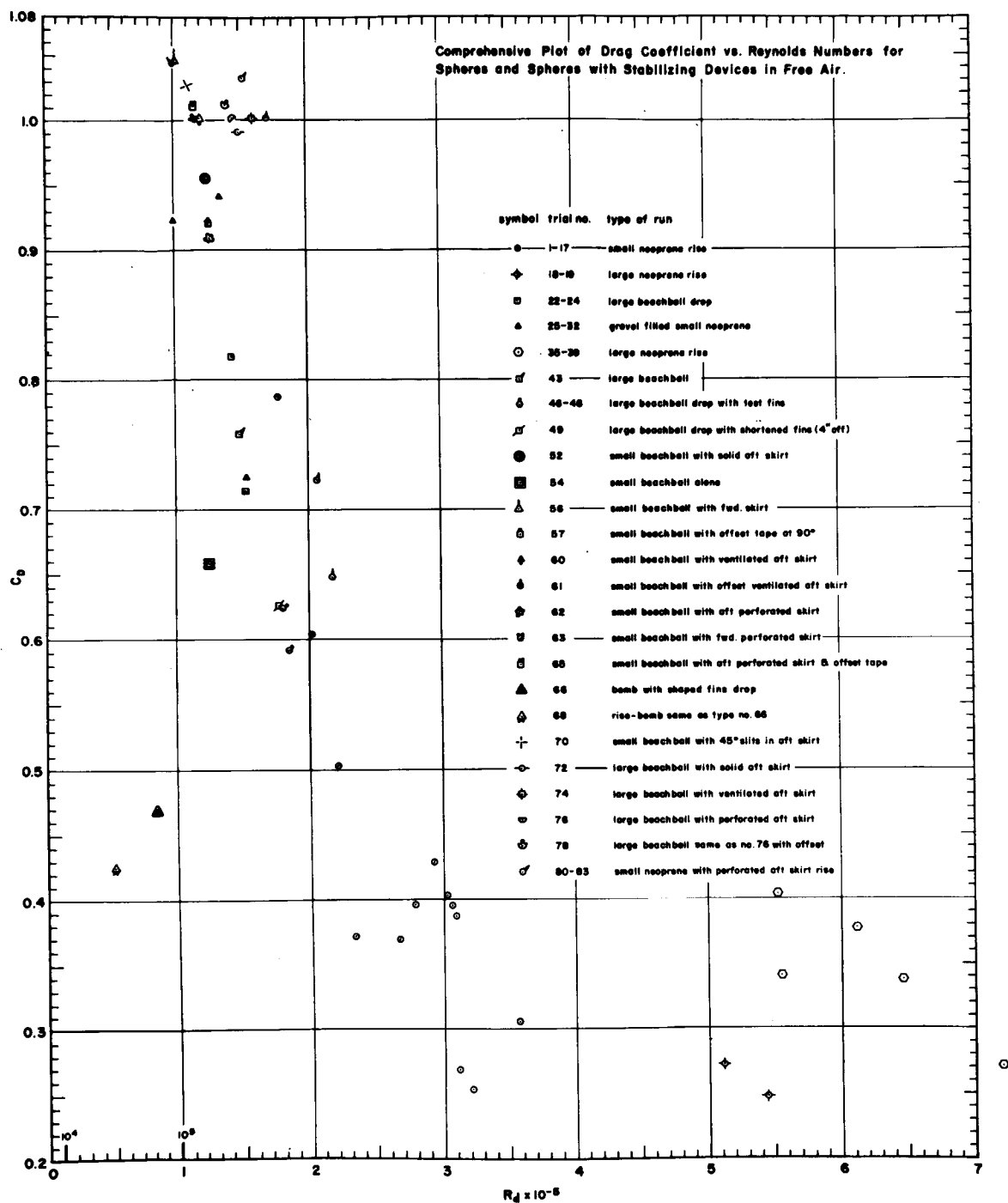


**FIGURE 10.  $C_D$  VERSUS  $R_d$  (Linear Plot) FOR SPHERES AND SPHERES WITH STABILIZING DEVICES IN FREE AIR**

## SECTION VII. CONCLUSIONS AND RECOMMENDATIONS

There have been two main successful approaches to obtaining high-resolution wind information with balloons:

- (1) Use the balloons at subcritical  $R_d$  where the lateral motions are small and regular and are effectively smoothed out in the smoothed FPS-16 data. This condition is manifested above about 11 km with the 2-meter diameter superpressure balloons, and the range can be extended downward by using smaller balloons with lower  $R_d$  because of their decreased vertical velocity and smaller diameter.
- (2) Stabilize the motions of balloons with supercritical  $R_d$  by adding roughness elements to increase the wake size, and/or by adding devices which keep the balloon in a constant orientation to the relative air flow or in a rotating motion about the vertical axis which averages out orientation effects.

Neither approach has yet given a complete, practical solution to the problem when considering the needs for simplicity and economy as well as fast ascent rate, broad altitude range capability, and short response distance.

The first method involves using a balloon which is small enough to have  $R_d < 200,000$  at the altitude of interest. In the practical case this involves the problem of obtaining a high altitude and a good ascent rate with balloons which are rather small. The difficulty should be somewhat ameliorated by using an expandable neoprene balloon, with radar chaff on its surface, rather than a fixed size superpressure balloon. The expandable balloon can cover a much greater altitude range and have a more constant vertical speed than can a fixed size balloon having the same  $R_d$  at a particular altitude. The expandable balloon will not be as exact a sphere as the superpressure one, but exact sphericity is probably not vital in the subcritical range. An additional simple feature which might help further is to add a small drag chute to help orient the balloon vertically. The chute will have its main stabilizing effect at low altitude where  $R_M$  is low and will also keep  $R_d$  slightly lower there but have negligible effect on vertical velocity and hence  $R_d$  at high altitudes after the balloon has expanded. The ideas presented here relating to the use of expandable balloons and drag chutes have not been verified by experimental data.

A solution fitting the second method is the Jimsphere (Scoggins, 1964), resembling somewhat the sphere with numerous large roughness elements shown in Figure 1-E. At sea level this version of the 2-meter balloon gives a motion with a small regular spiral, small enough to yield smooth data with the FPS-16. Another approach to stabilizing the wake configuration of a superpressure balloon would be to (a) orient the balloon vertically with a small drag chute at least 10d back, (b) trip the wake separation at a specific point by a belt with vortex generators (merely 2-inch x 2-inch plates angled to the flow) around the equator, and (c) obtain rotation to cancel asymmetries by some rotation vanes at the equator (or by having most of the plates angled one way).

The response distances of practical size balloons tend to be short enough for average applications. Fortunately the methods giving high drag or low  $R_d$  tend to give short response distances

All the methods discussed still apparently involve a small-amplitude spiral motion of the ascending balloon, small enough to be lost in the smoothing required with FPS-16 tracking data, but appreciable if optical tracking or Doppler radar is employed to give turbulence spectra.

Extrapolating the pool tests at subcritical  $R_d$  to the case of a 2-meter superpressure sphere also at subcritical  $R_d$  above 11 km, taking  $RM = 0.5$  and using the "motion magnitude vs  $RM$ " curve of Figure 3, implies that in still air the balloon will move a total of about 2 m to the right and then 2 m to the left (with a 20 m wave length), for an RMS movement of 0.58 m. To smooth out the radar-induced noise, the radar data (0.1 second positions) are averaged over 4 sec. This averaging also effectively removes the periodic balloon motion. If the averaging time corresponds to 1 or 2 wave lengths, the indicated balloon motion in still air is zero; if the averaging time corresponds to 1-1/2 wave lengths, the RMS indicated balloon motion in still air is still only about 0.07 m.

The water experiments discussed here apparently give results which are generally consistent with the measurements on balloons in the atmosphere. It would be fruitful to perform similar water tests in a more refined manner, with (a) a deeper tank to permit the larger spheres to attain true equilibrium motion and to permit the use of

large enough spheres to give higher  $R_d$ , (b) a bigger selection of spheres to cover broad ranges of  $RM$ ,  $R_d$ , and smoothness while holding one parameter constant at a time, and (c) more attention to the details of the lateral motions and the flow field.

#### ACKNOWLEDGMENTS

The authors are indebted to Mr. Neil Kelley and Mr. Ira Dehimy of MRI who constructed the test devices and handled much of the experimental testing. Mr. Harold Musselman of California Institute of Technology made available the C.I. T. Gymnasium for the indoor tests, which materially aided the program. Mr. James Scoggins of Marshall Space Flight Center has helped the study greatly through discussions and by providing various data on ascents of spherical and non-spherical balloons.

## REFERENCES

- Bacon, David L., and Elliott G. Reid, 1924: NACA Report No. 185, pp. 471-487.
- Henry, Robert M., and James R. Scoggins, 1963: Self-induced balloon motions. *Astronautics and Aerospace Engineering*, October, p 5.
- Hirsch, P., 1924: Motion of spheres in still fluids (from *Zeitschrift für Angewandte Mathematik und Mechanik*, Vol. III, No. 2, pp 93-107, April, 1923), NACA Technical Memorandum No. 257, translation.
- Hoerner, S., 1935: Tests of spheres with reference to Reynolds number, turbulence, and surface roughness. NACA Technical Memorandum No. 777.
- Killen, Gwendolyn L., 1960: Balloon behavior experiments. USASRDL Tech. Report 2093, DA TASK NR. 3D36-04-001-01, Ft. Monmouth, N. J.
- Lunnon, R. G., 1925: Fluid resistance to moving spheres. *Proc. Royal Society "A"*, Vol. 110, pp 302-326.
- \_\_\_\_\_, 1928: Fluid resistance to moving spheres. *Proc. Royal Society "A"*, Vol. 118, pp 608-694.
- Millikan, C. B., and A. L. Klein, 1933: The effect of turbulence - an investigation of maximum lift coefficient and turbulence in wind tunnels and in flight. *Aircraft Engineering*, August, pp 169-174.
- Murrow, H. N., and R. M. Henry, 1964: Self-induced balloon motions and their effects on wind data. Paper presented at the AMS 5th Conf. on Applied Meteorology, Atlantic City, Mar. (NASA-Langley).
- Reed, Wilmer H., III, and James W. Lynch, 1963: A simple fast response anemometer. *J. Appl. Meteor.*, 2, 3, pp 412-416.
- Reid, D. F., 1964: The ROSE wind sensor. Paper presented at the AMS 5th Conf. on Applied Meteorology, Atlantic City, March. (AFCRL).

- Scoggins, J.R., 1964: Spherical balloon wind sensor behavior.  
Paper presented at the AMS 5th Conf. on Applied Meteorology,  
Atlantic City, March. (NASA-Huntsville, Marshall Space Flight  
Center).
- Stinson, R.L., A.I. Weinstein, and E.R. Reiter, 1964: Details of  
wind structure from high resolution balloon soundings. Revision  
of Final Report to NASA, Marshall Space Flight Center,  
Huntsville, Alabama, under Contract NAS 8-5294.  
(MRI64 FR-123a) Meteorology Research, Inc. Published  
as NASA TM X-53115, dated August 24, 1964.

July 27, 1964

APPROVAL

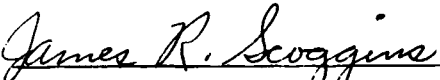
TM X-53089

STUDY OF SPHERE MOTIONS AND BALLOON WIND SENSORS

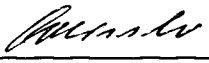
By Paul B. MacCready, Jr. and Henry R. Jex

The information in this report has been reviewed for security classification. Review of any information concerning Department of Defense or Atomic Energy Commission programs has been made by the MSFC Security Classification Officer. This report, in its entirety, has been determined to be unclassified.

This document has also been reviewed and approved for technical accuracy.

  
\_\_\_\_\_  
JAMES R. SCOGGINS  
Chief, Environmental Applications Group

  
\_\_\_\_\_  
WILLIAM W. VAUGHAN  
Chief, Aero-Astrophysics Office

  
\_\_\_\_\_  
E. D. GEISSLER  
Director, Aero-Astrodynamic Laboratory

## ERRATA

NASA TECHNICAL MEMORANDUM X-53089

### STUDY OF SPHERE MOTION AND BALLOON WIND SENSORS

By Paul B. MacCready, Jr. and Henry R. Jex\*

\* Prepared by Meteorology Research, Inc. for Aero-Astroynamics Laboratory

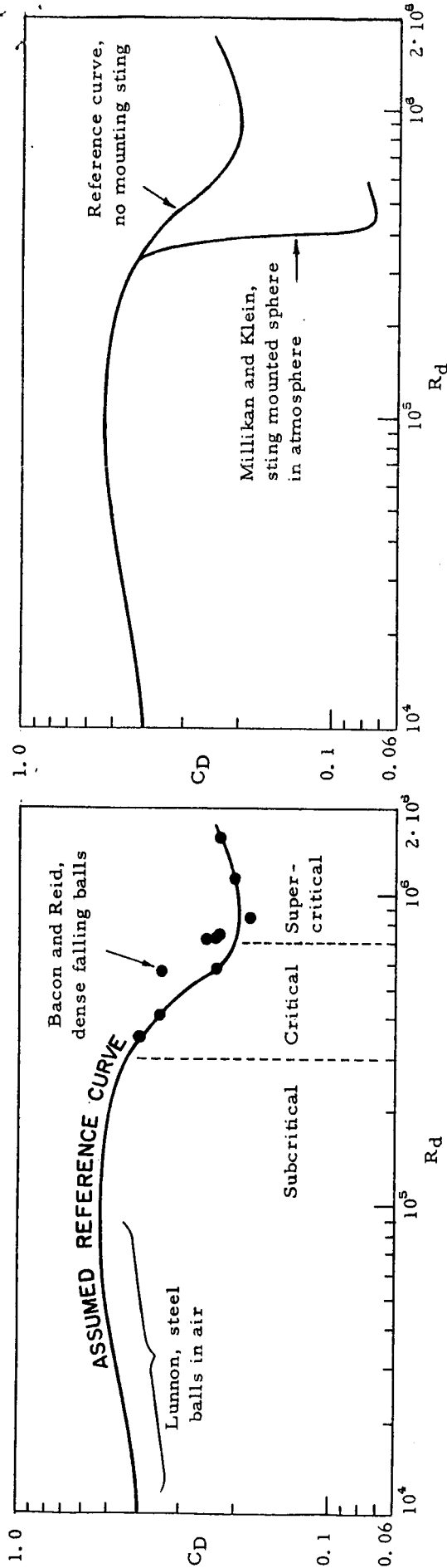
Page 9, Figure 2: In Figure 2c there is some coordinate labeling missing or erroneous and the small roughness curve has been corrected.

Replace Figure 2 with the corrected Figure 2 which is attached.

Page 13: Delete the fourth sentence of the second paragraph. (Very large roughness increases the turbulent separation at large  $R_d$  so much that  $C_D$  is near subcritical value (for smooth spheres), while at  $R_d$  large roughness will stabilize and reduce the wake and give  $C_D$  comparable to, or even less than, rigidly mounted spheres having laminar separation.) The sentence is correctly written as:

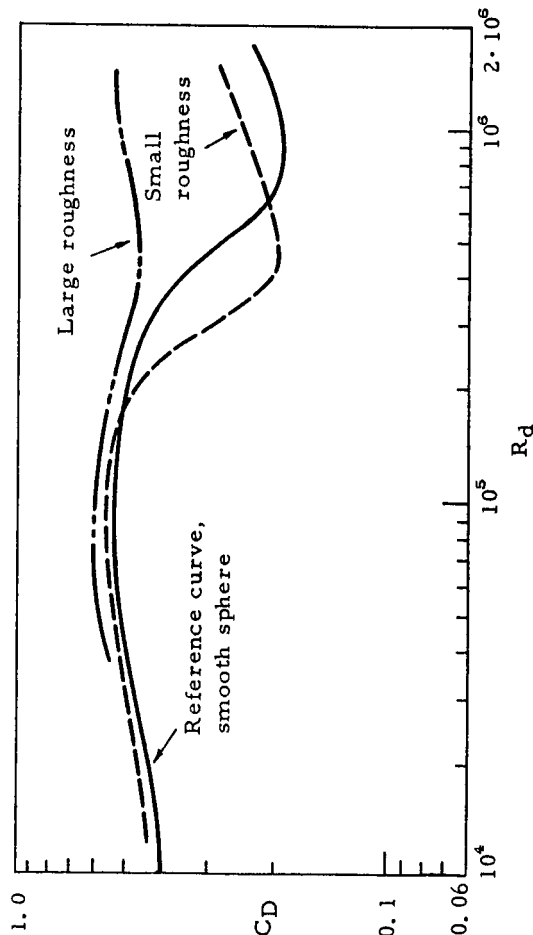
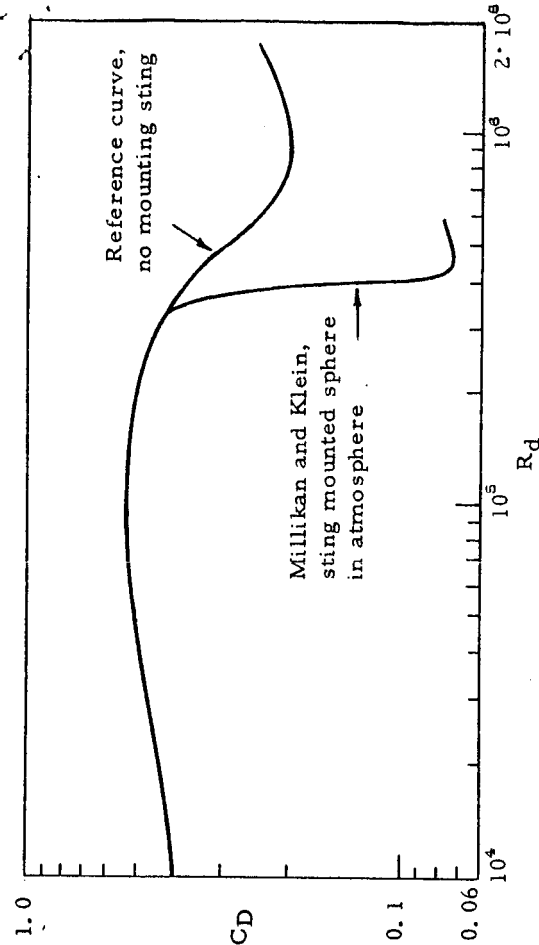
Very large roughness increases the turbulent separation at large  $R_d$  so much that  $C_D$  is near subcritical value (for smooth spheres); at subcritical  $R_d$  large roughness will stabilize and reduce the wake and give  $C_D$  comparable to, or even less than, rigidly mounted spheres having laminar separation.



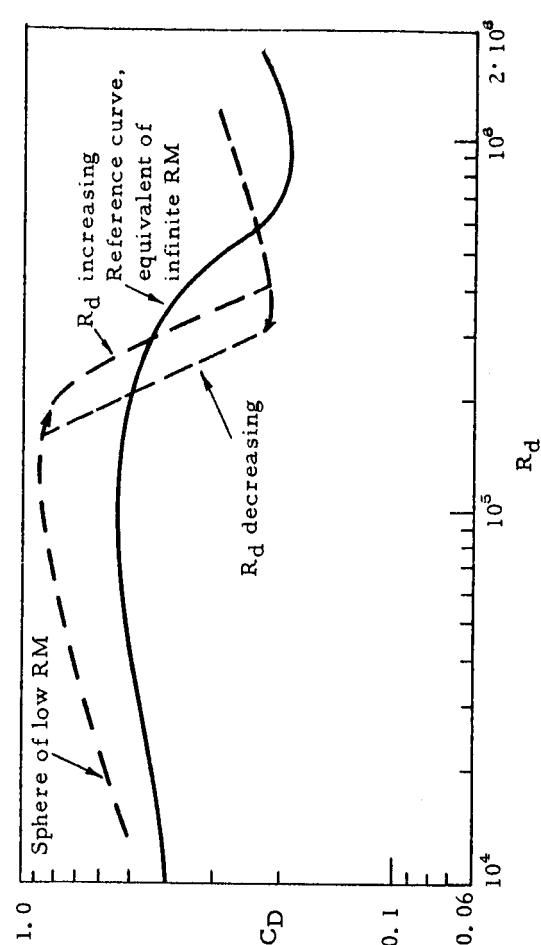


A. Reference curve for spheres of very high relative mass.

B. Effect of a sting mount on drag.



C. Effect of roughness on drag (high relative mass).



D. Effect of low relative mass (permitting lateral motion).

Fig. 2. SUMMARY OF PHYSICAL EFFECTS ON  $C_D$  VERSUS  $R_d$  REPRESENTATION